Supplementary material

Mamad et al 2017

- **Supplementary Figures 1-9**
- **Supplementary Table 1**
- **Supplementary Movies 1-5**

Supplementary Figure 1:

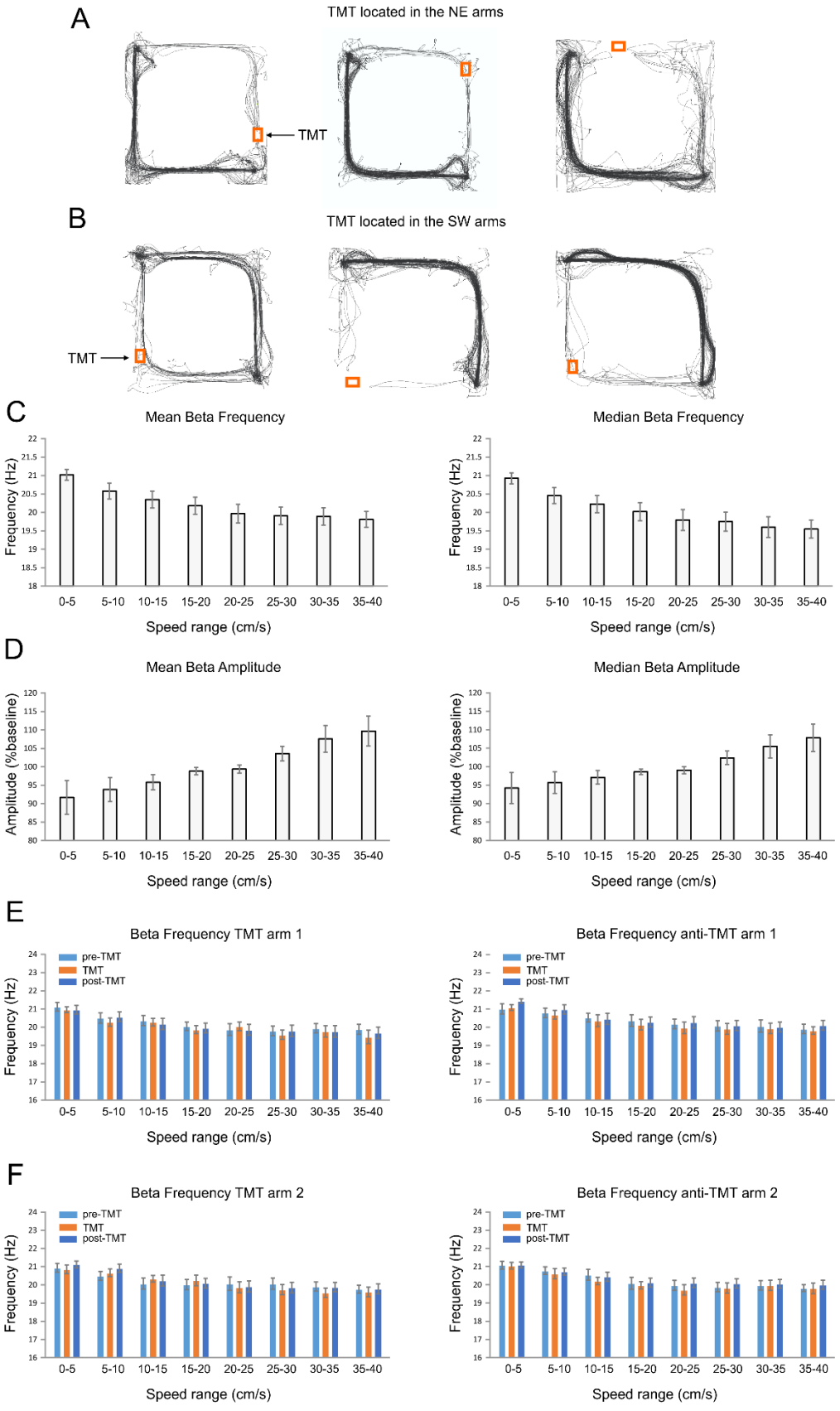

Supplementary Figure 1. **Hippocampal beta frequency and amplitude depend on whole body motion.** (A) Navigation path of three animals during the TMT session with TMT odor applied in the northeast (NE) arms of the track. (B) Navigation path of three animals during the TMT session with TMT odor applied in the southwest (SW) arms of the track. (C) Mean (left panel) and median values (right panel) of beta frequency measured during different whole body speed ranges of 0 – 40 cm/s in bins of 5 cm/s. (D) Mean (left panel) and median values (right panel) of beta amplitude (percent of baseline) measured during different speed ranges of 0 – 40 cm/s in bins of 5 cm/s. Error bars, mean ± s.e.m. (E) Beta frequency for TMT arm 1 (left), anti-TMT arm 1 (right), (F) TMT arm 2 (left), and anti-TMT arm 2 (right). The frequency values (Hz) are presented as a function of the animal's speed, where beta amplitude is evaluated for speed range of 0 – 40 cm/s in bins of 5 cm/s. Error bars, mean ± s.e.m.

Supplementary Figure 2:

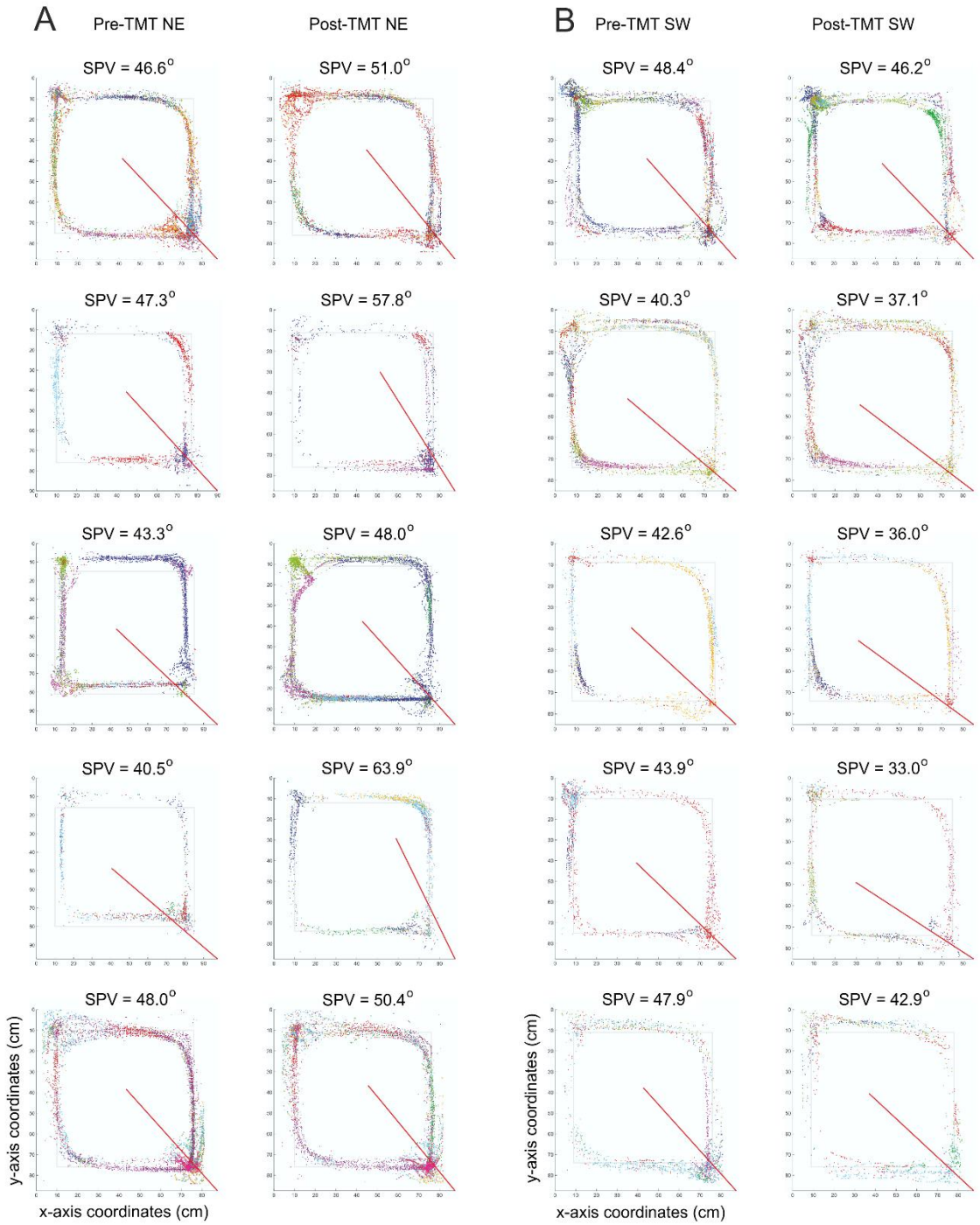

Supplementary Figure 2. TMT-evoked shift of the spatial population vector. (A) Spatial distribution of the spikes (colored dots) of CA1 place cells (represented by different colors) recorded during pre-TMT (left panel) and post-TMT recording session (right panel) from five animals from the NE-group. The straight red line denotes the weighted spatial population vector (SPV) between SW at 0° and NE at 90°. (B) Spatial distribution of the spikes (colored dots) of CA1 place cells (represented by different colors) recorded during pre-TMT (left panel) and post-TMT recording session (right panel) from five animals from the SW-group. The straight red line denotes the weighted SPV between SW at 0° and NE at 90°.

Supplementary Figure 3:

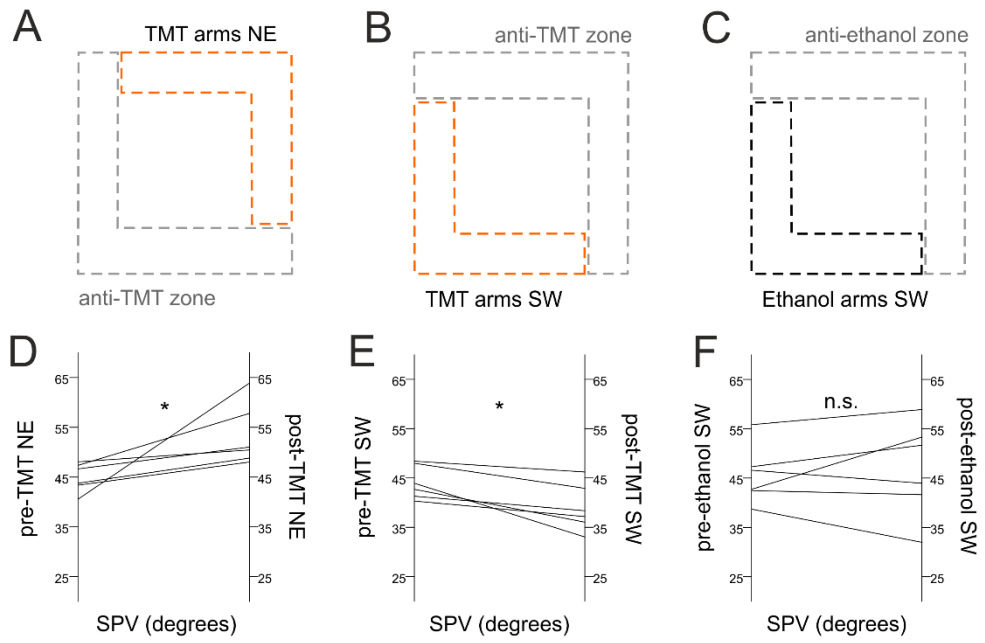

Supplementary Figure 3. Aversion experience directs the bias of the spatial population vector. (A) Schematic representation of the TMT arms position (marked with red) in the rectangular-shaped linear track for the NE group of animals and (B) for the SW group of animals. (C) Schematic representation of the ethanol arms position (marked with black) for the control group of animals. (D) Comparison of the pre- and post-TMT weighted SPV between NE- (E) SW- and (F) control group of animals. For the control experiments filter paper scented with 10% ethanol were positioned in the SW arms of the track. The rats were habituated to the ethanol odor prior the recording sessions.

Supplementary Figure 4:

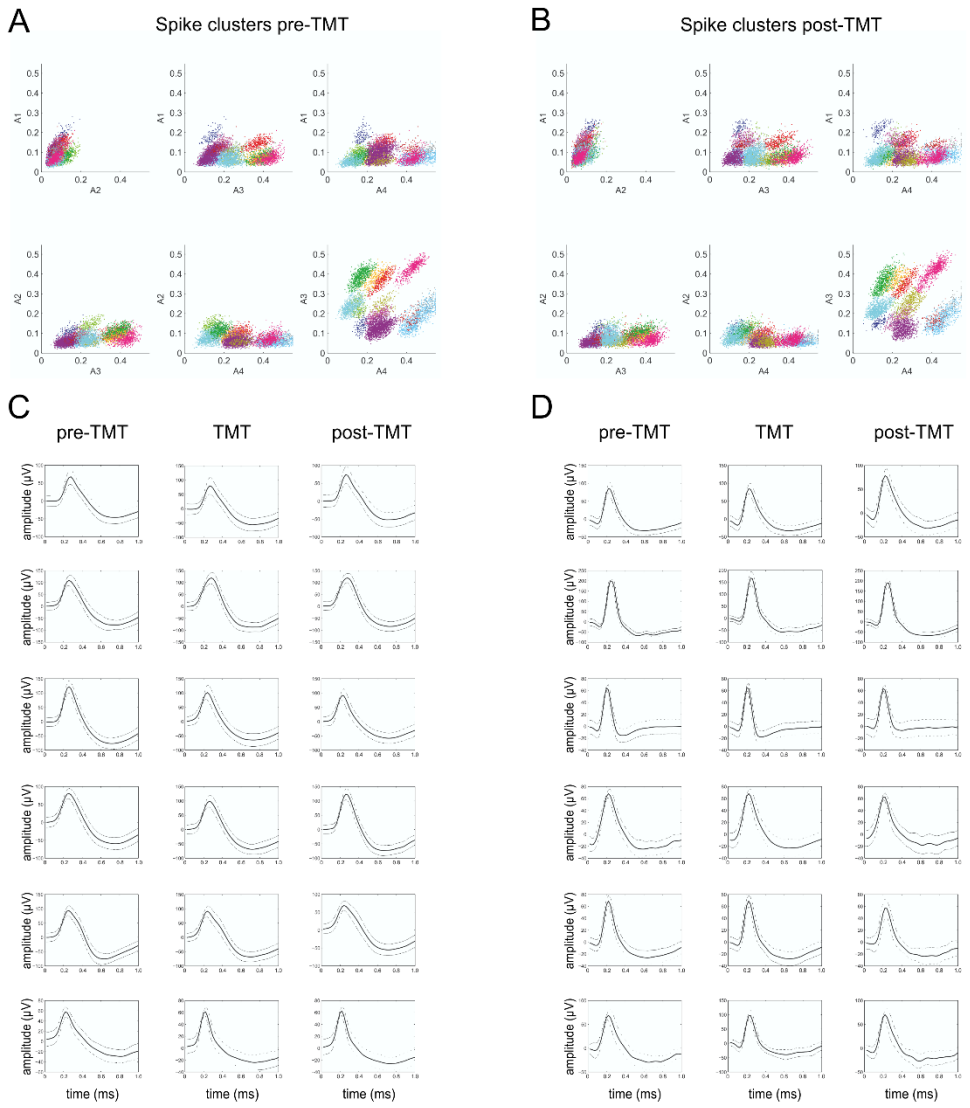

Supplementary Figure 4. Stability of the recorded signals across subsequent recording sessions. (A) Scatterplot, showing the signals from multiple units recorded between each pair of electrodes on a given tetrode from a pre-TMT session. Each tetrode measures the signal amplitude from four electrodes (A1-A4). The color-coded clusters represent the spikes from individual units at the scatterplot. (B) Scatterplot, showing the same signals recorded from a post-TMT session. (C) Waveforms of the place cell shown in Fig. 3D, recorded from the pre-TMT (left), TMT (middle) and post-TMT session (right). The solid line shows the average waveform shape; the dashed lines show the 1 SD confidence intervals. (D) Waveforms of the

place cell shown in Fig. 3E, recorded from the pre-TMT (left), TMT (middle) and post-TMT session (right). The solid line shows the average waveform shape; the dashed lines show the 1 SD confidence intervals.

Supplementary Figure 5:

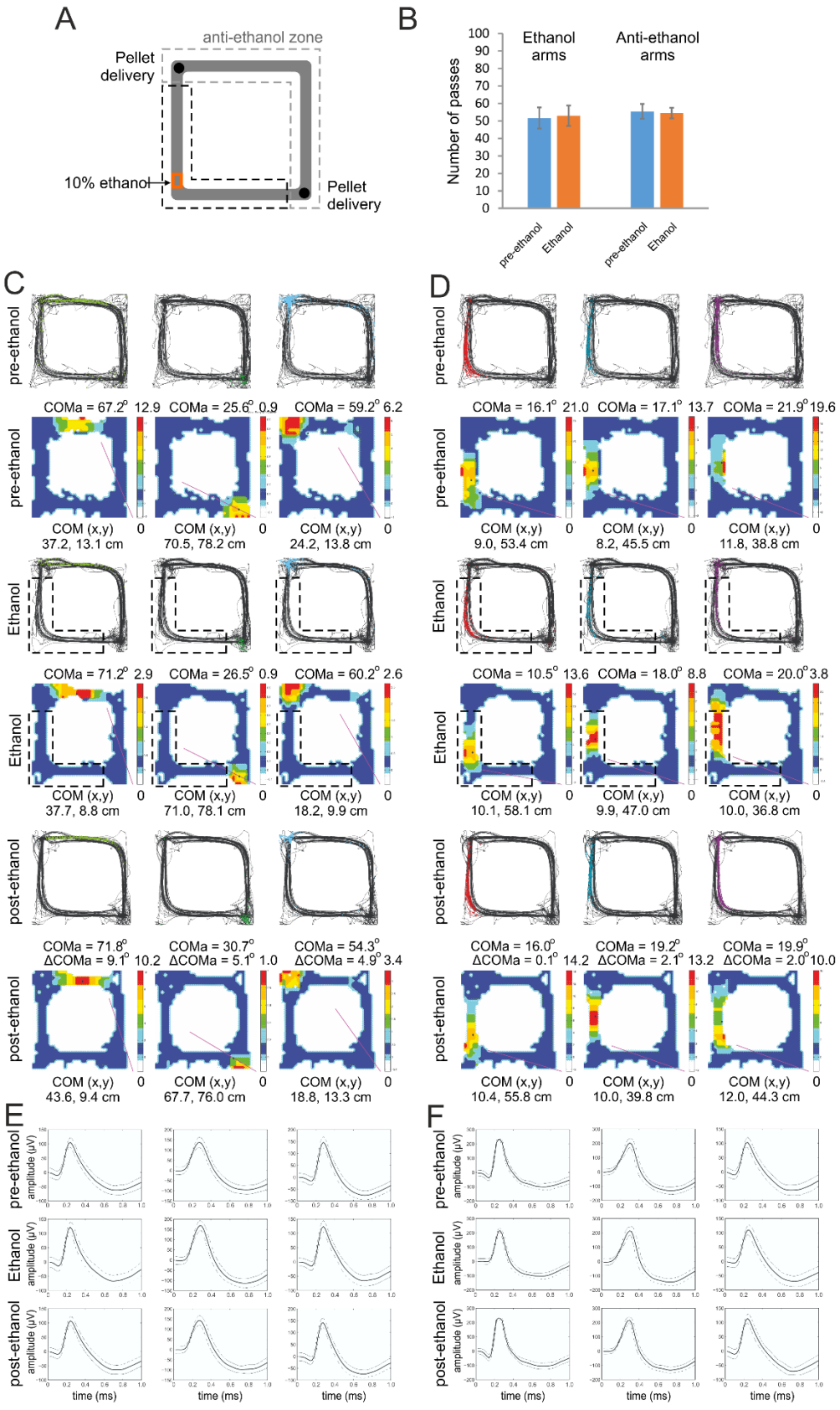

Supplementary Figure 5. Place field stability in control conditions. (A) Schematic representation of the application of a familiar neutral scent, 10% ethanol (marked with red) in the SW arms of rectangular-shaped linear track for the control group of animals. (B) Number of passes through the ethanol arms (left) and anti-ethanol arms (right) for the control group of rats, before (blue) and during (red) the odor exposure. Error bars, mean ± s.e.m. (C) Three place fields from sample animal with fields located outside the ethanol arms during pre- (top), ethanol (middle) and post-ethanol sessions (bottom). For each session the upper panels show the animal trajectory with spikes, marked with colored dots, while the lower panels show color-coded firing rate. (D) Three place fields from same animal with fields located inside the ethanol arms during pre- (top), ethanol (middle) and post-ethanol sessions (bottom). For each session the upper panels show the animal trajectory with spikes, marked with colored dots, while the lower panels show color-coded firing rate. (E) Waveforms of the place cells shown in C, and (F) waveforms of the cells shown in D, respectively. The solid line shows the average waveform shape; the dashed lines show the 1 SD confidence intervals.

Supplementary Figure 6:

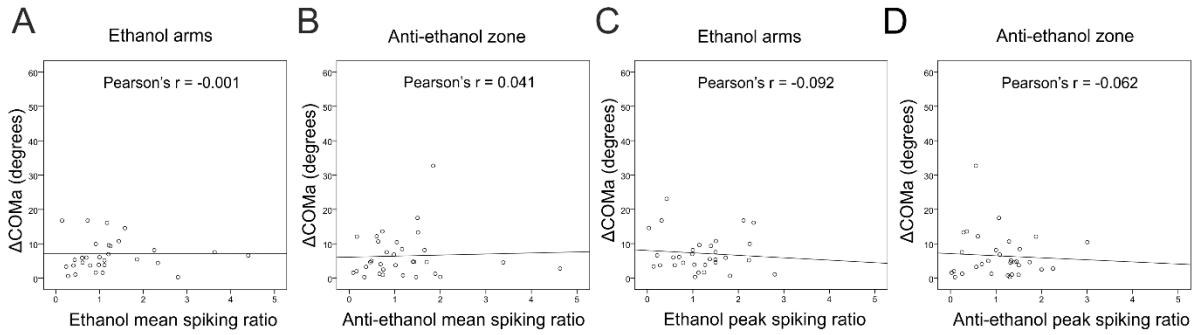

Supplementary Figure 6. The center of mass shift and place cells' spiking do not correlate after exposure to non-aversive odor. (A) Correlation between ΔCOMa and the spiking ratio based on the mean firing rate of the place cells' spikes in the ethanol arms. (B) Correlation between ΔCOMa and the spiking ratio based on the mean firing rate of the place cells' spikes in the anti-ethanol zone. (H) Correlation between ΔCOMa and the spiking ratio based on the peak firing rate for the spikes in the ethanol arms. (I) Correlation between ΔCOMa and the spiking ratio based on the peak firing rate for the spikes in the anti-ethanol zone.

Supplementary Figure 7:

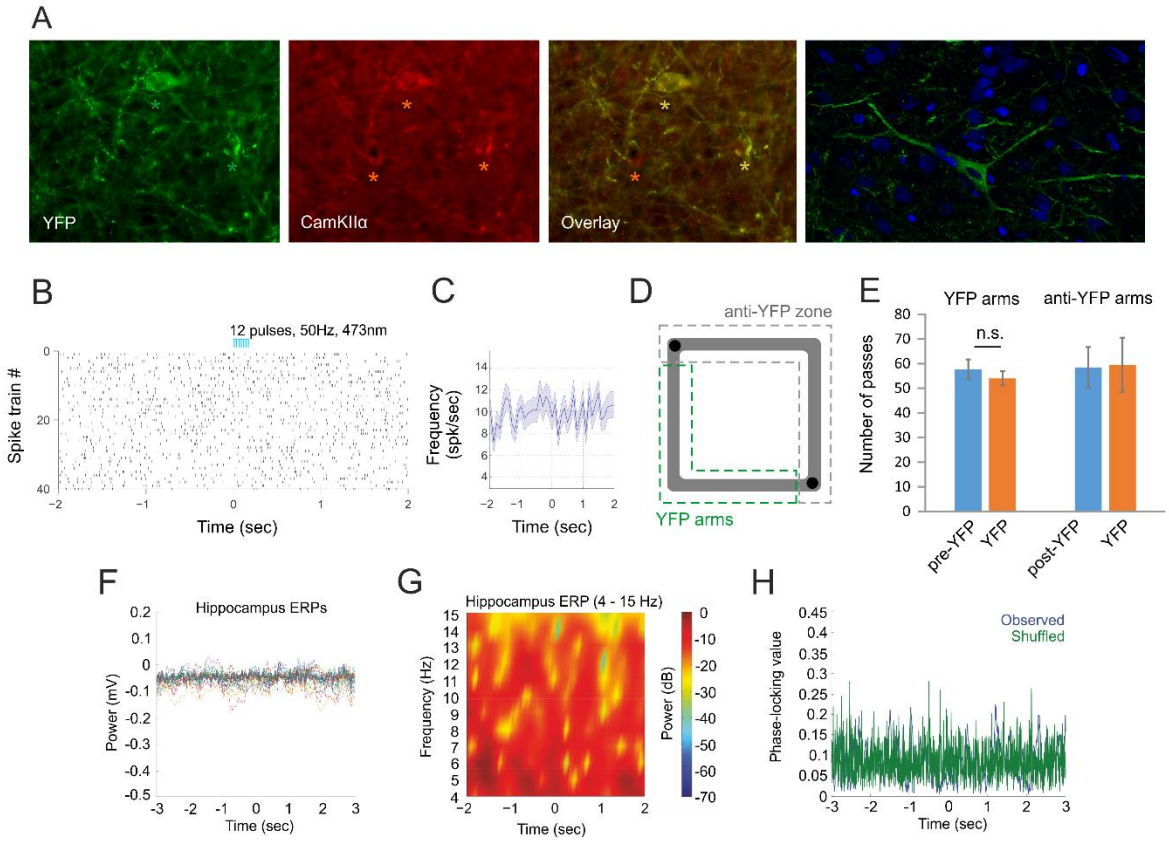

Supplementary Figure 7. Photostimulation of control YFP neurons in the basolateral complex of amygdala. (A) YFP expression (left), anti-calcium/calmodulin-dependent protein kinase II alfa (anti-CamKIIα) staining (middle) and their overlay in BLA (right). The green asterisks show two YFP-expressing neurons, while the red asterisks show three CamKIIα-marked neurons. The confocal image on the far right shows YFP-expressing neurons (green) in BLA is histology with DAPI staining (blue). Raster plot from 40 repetitions (B) and (C) firing frequency of time-locked photostimulation of a BLA cell in control animals injected with AAV-YFP viral construct. Time 0 indicates the delivery of the first train of the stimulation protocol. (D) Experimental setup: light delivery in the south and west arms of the rectangular-shaped linear track (YFP arms, marked with dashed green line). No photostimulation was applied in the anti-ChR2 zone (marked with dashed gray line). (E), Number of passes counted from control animals injected with AVV-YFP construct in the YFP arms vs anti-YFP zone

during the pre-YFP, YFP-, and post-YFP sessions. Error bars, mean ± s.e.m. (F) Event related potentials (ERPs) recorded in dorsal CA1 from of 32 electrodes in a sample control animal. Time 0 indicates the delivery of the onset of the BLA YFP photostimulation. (G) Color-coded power spectrogram of hippocampal low-frequency oscillations (4 – 15Hz) during the YFP photostimulation. (I) Representative phase-locking value after BLA YFP photostimulation for the observed data (blue) and for control shuffled data (green).

Supplementary Figure 8:

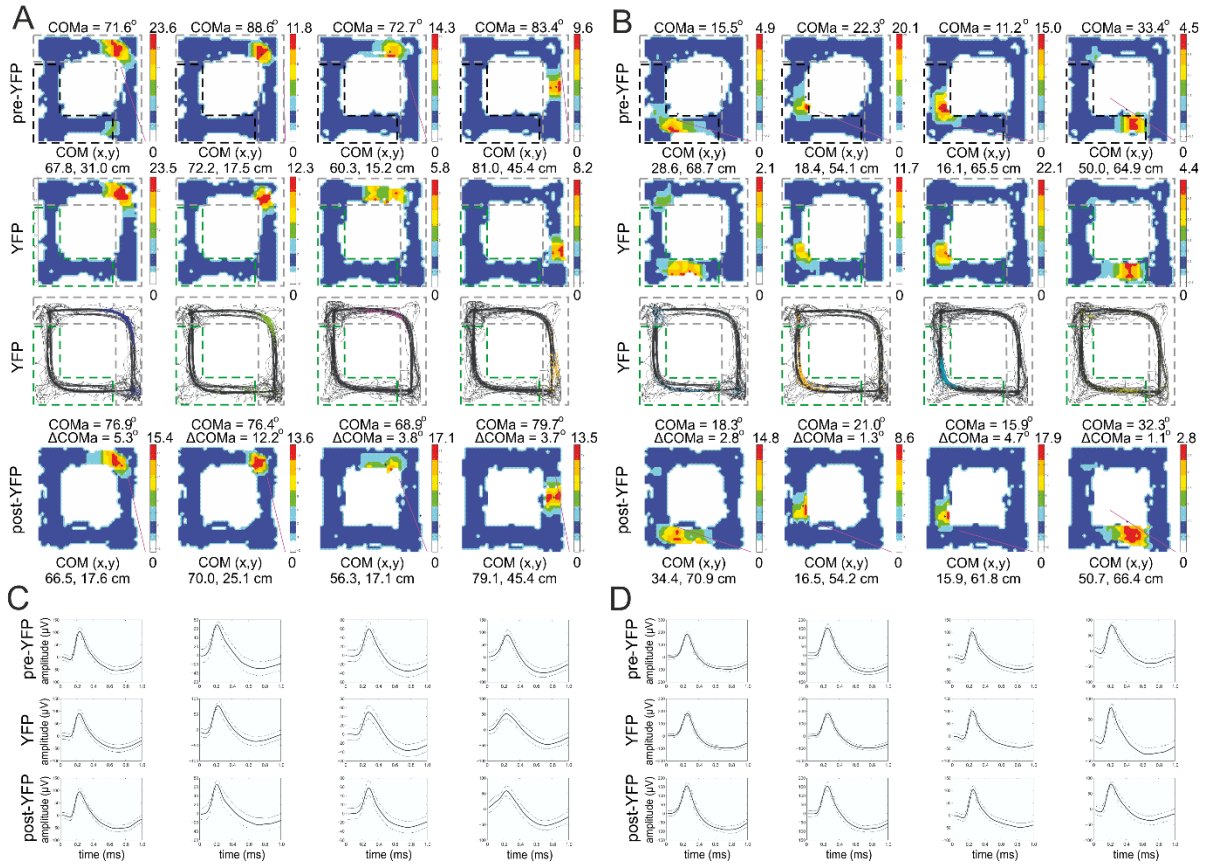

Supplementary Figure 8. Comparison between intra- and extra-field place cells spiking for control YFP rats. (A) Four place fields from two sample animals with fields located outside the YFP arms during pre-YFP sessions (top), YFP (middle) and post- YFP sessions (bottom). For the YFP session the upper panels show maps with color-coded firing rate, while the lower panels show the animal trajectory with spikes, marked with colored dots. (B) Four place fields from the same two animals with fields located inside the YFP arms during pre-YFP sessions (top), YFP (middle) and post-YFP sessions (bottom). For the YFP session the upper panels show maps with color-coded firing rate, while the lower panels show the animal trajectory with spikes, marked with colored dots. (C) Waveforms of the place cells shown in A, and (D) waveforms of the cells shown B, respectively. The solid line shows the average waveform shape; the dashed lines show the 1 SD confidence intervals.

Supplementary Figure 9:

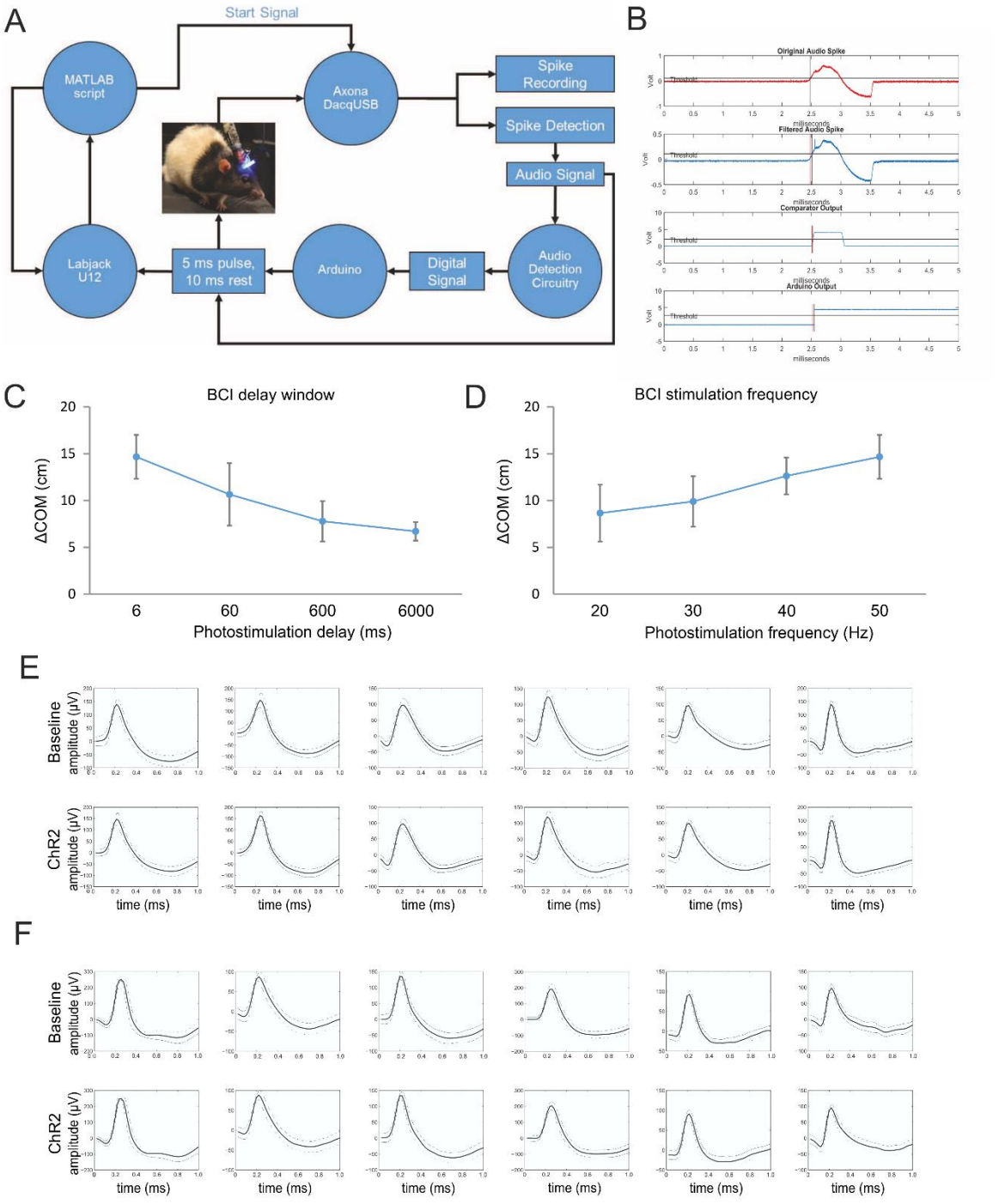

Supplementary Figure 9. Closed-loop light delivery with brain-computer interface. (A) Detailed BCI schematics. The signal from the headstage was processed to 1) Preamp/ADC unit with differential amplifiers and analogue to digital converter; 2) system unit (Axona Ltd.) with digital signal processing (DSP) microprocessor; 3) computer with installed DacqUSB system

(Axona Ltd.), which enables audio monitoring of the spikes detected during single-unit recording; 4) The comparator circuit is composed of an operational amplifier for threshold-dependent square pulse generation; 5) Arduino UNO board (Arduino) with a microcontroller programmed to operate in a loop detecting a high digital input from the comparator; 6) blue light laser for photostimulation (5ms pulse width and 10ms post-stimulation pause) with a parallel output towards data acquisition system; 7) data acquisition system (Labjack U12) recorded the onsets of the stimulation modulation pulses produced by the Arduino board to compare the matching of the stimulation signal to the recorded single-unit spikes; 8) In-house scripts written on MATLAB (MathWorks, Inc., USA) determined the percentage of the stimulation pulses that were triggered by the recorded spikes from chosen place cell and the percentage of the spikes from the chosen place cell that successfully evoked stimulation pulses. (B) Circuit delays of 39.5 (± 22.9) μs for the low pass filter between the input and the output of the non-filtered and filtered audio spike when reaching the threshold value (upper two panels), and delays of 12.9 (± 2.4) μs for the comparator processing, and 32.4 (± 4.7) μs for the Arduino UNO board processing (lower two panels). (C) Exponential dependence of ΔCOM on the BCI delay: 14.66 ± 2.34 for delay below 6 ms; 10.56 ± 3.33 for delay of 60 ms; 7.78 ± 2.15 for delay of 600 ms, and 6.70 ± 0.98 for delay of 6000 ms (n = 12 cells). Error bars, mean ± s.e.m. (D) Decimal dependence of ΔCOM on the BCI stimulation frequency: 8.65 ± 3.04 for frequency of 20Hz; 9.89 ± 2.70 for frequency of 30Hz; 12.62 ± 1.97 for frequency of 40Hz, and 14.66 ± 2.34 for frequency of 50Hz (n = 12 cells). Error bars, mean ± s.e.m. (E) Waveforms of the non-BCI cells shown in Fig. 10B, recorded from the baseline (upper row), and ChR2 session (lower row). (F) Waveforms of the non-BCI delayed cells Fig. 10D, recorded from the baseline (upper row), and ChR2 session (lower row). The solid line shows the average waveform shape; the dashed lines show the 1 SD confidence intervals.

Supplementary Table 1. CA1 place field reconfiguration after instant and delayed BCI photostimulation of BLA fibers.

Baseline				ChR2 BCI instant				Difference	
Cell	COMa degree	COM x cm	COM y cm	Cell	COMa degree	COM x cm	COM y cm	dCOM cm	|dCOMa| degree
1	50.9	43.0	34.7	1	70.9	46.8	11.5	23.5	19.9
2	48.4	52.0	47.0	2	67.7	46.8	15.9	31.6	19.3
3	31.6	30.5	51.2	3	27.2	25.4	53.0	5.4	4.3
4	36.6	31.5	42.7	4	55.8	47.2	31.6	19.3	19.1
5	57.2	26.6	16.7	5	44.1	20.0	20.6	7.7	13.1
6	32.4	28.9	46.7	6	38.0	45.2	54.4	18.0	5.6
7	29.0	38.3	61.2	7	37.7	38.8	50.5	10.7	8.7
8	88.0	69.1	15.3	8	77.4	63.6	17.1	5.8	10.5
9	70.4	70.8	41.9	9	45.0	60.8	60.8	21.4	25.4
10	68.1	30.7	10.1	10	63.1	22.6	10.6	8.1	5.0
11	62.9	60.2	31.5	11	52.4	52.7	40.1	11.3	10.5
12	21.4	14.2	45.3	12	32.1	27.4	44.9	13.2	10.7
Baseline				ChR2 BCI delayed 6 sec				Difference	
Cell	COMa degree	COM x cm	COM y cm	Cell	COMa degree	COM x cm	COM y cm	dCOM cm	|dCOMa| degree
1	36.0	26.0	36.2	1	37.3	27.4	36.2	1.4	1.3
2	47.7	67.7	72.0	2	34.9	72.8	77.5	7.5	12.8
3	65.0	40.5	17.0	3	58.7	37.7	22.2	5.9	6.2
4	60.4	61.1	41.1	4	58.7	61.9	45.0	4.0	1.7
5	47.3	38.3	35.4	5	39.4	32.4	39.7	7.3	7.8
6	61.2	63.5	44.0	6	66.4	66.4	41.6	3.8	5.2
7	71.7	67.6	33.2	7	79.1	70.0	31.4	3.0	7.4
8	56.1	58.1	43.2	8	49.8	55.1	48.7	6.3	6.3
9	12.4	35.4	72.4	9	22.3	45.5	70.7	10.3	9.8
10	51.9	31.3	24.4	10	43.9	30.3	31.5	7.2	8.0
11	31.5	26.6	44.9	11	40.6	39.3	46.0	12.7	9.1
12	62.2	51.8	25.6	12	66.8	45.3	16.6	11.1	4.6

Supplementary Movie 1: TMT-induced aversion. Navigation in rectangular-shaped linear track of rat with chronically-implanted tetrodes in the hippocampal CA1 region. The animal was trained to navigate between the southwest and northeast corners, where two pellets were continuously positioned. TMT was placed in particular location of the track, which is denoted in red.

Supplementary Movie 2: ChR2-induced aversion. Navigation in rectangular-shaped linear track of rat with chronically-implanted tetrodes in hippocampus. The first half of the video shows pre-ChR2 session, measuring baseline behavioral and electrophysiological activity signals. The second half of the video shows light delivery, triggering photoexcitation of BLA neurons. The coordinates of photostimulation (ChR2 arms) are denoted in blue.

Supplementary Movie 3: ChR2-induced aversion. Pre-ChR2 and ChR2 sessions for second animal.

Supplementary Movie 4: Extra-field spiking during ChR2 photostimulation of BLA. Analysis software visualization of the animal's path (marked with black line) and the recorded place cell's spiking (denoted with purple dots). The represented speed is 2x real-time. The first half of the video shows 238 seconds of pre-ChR2 session, followed by images of the raw signal and the firing map for the entire 12 minutes baseline session. The second half of the video shows 238 seconds of ChR2 session, followed by images of the raw signal and the firing map for the entire 12 minutes ChR2 session. The coordinates of photostimulation (ChR2 arms) are denoted in blue.

Supplementary Movie 5: BCI-triggered ChR2 photostimulation of BLA. Navigation in rectangular-shaped linear track of rat with tetrodes implanted in the hippocampal CA1 region. The first half of the video shows pre-ChR2 session, measuring baseline behavioral and electrophysiological activity signals. The inset shows the spikes recorded from four tetrodes.

A tetrode channel was chosen for audio signal generation and BCI processing. The white square denotes the channel from which the signal was selected to evoke the laser pulses. The second half of the video shows spike-triggered BCI light delivery, triggering photoexcitation of BLA neurons.